The effects of road curvature on the stability of path-following of automated vehicles

Illés Vörös[1,2] and Dénes Takács[1,2]

[1] Department of Applied Mechanics, Faculty of Mechanical Engineering,
Budapest University of Technology and Economics, Műegyetem rkp. 3., H-1111
Budapest, Hungary
[2] ELKH-BME Dynamics of Machines Research Group, Budapest University of
Technology and Economics, Műegyetem rkp. 3., H-1111 Budapest, Hungary

Abstract. The stability analysis of a path-following controller for automated vehicles is presented, with the consideration of path curvature and feedback delay. The analysis is based on a kinematic vehicle model expressed in a path reference frame. The steering controller includes feedforward and feedback terms, and the time delay in the control loop is also considered. The effects of the path curvature are analyzed using compact analytical expressions, stability charts and numerical simulations. The results help the designer select the optimal control gains and the limitations of tuning the controller with the assumption of a straight-line reference path are also shown.

Keywords: vehicle dynamics, time delay, lane-keeping control, steering control, stability

1 Introduction

Designing stable and safe path following controllers with sufficiently high performance is a crucial step towards vehicle automation and it is also a cornerstone of many advanced driver assistance systems, such as lane-keeping and lane changing control. There are many different approaches to design the corresponding controllers, from simple geometrical considerations to machine learning-based methods [1]. The designed controller must be able to maintain its performance and stability under a variety of circumstances: the controlled vehicle must be able to handle unexpected disturbances such as road surface irregularities and suddenly appearing obstacles [2], the variation of the road curvature [3], as well as sensor uncertainties and noise. In addition, the feedback delay in the control loop has also been shown to greatly impact the performance of path following [4].

In this study, the analysis of a steering controller for path following is presented, with the consideration of time delay in the control loop and the curvature of the reference path. The calculations are based on a kinematic single-track vehicle model and a constant path curvature, which allows us to present the results in the form of compact analytical expressions. The constraint forces at the wheels are also calculated to ensure that loss of traction does not occur. We derive compact analytical expressions for the stability boundaries and optimal control gains, and present the results using stability charts and numerical simulations. Our results show the benefits of taking into account the path curvature when tuning the controller, especially in the case of highly dynamic maneuvers.

The rest of the paper is organized as follows: Section 2 presents the derivation of the vehicle model both in a global coordinate system and a path reference frame. The path following controller is introduced in Section 3, while the stability analysis is performed in Section 4. The results are concluded in Section 5.

2 Vehicle model

The vehicle model considered in this study is an in-plane, single-track (bicycle) model (see Fig. 1), where the vehicle is modeled with respect to its longitudinal axis, and the roll, pitch and vertical dynamics are neglected. Furthermore, we assume that no tire deformation occurs at the wheels, i.e. the tire side slip angles remain zero.

The vehicle parameters consist of the wheelbase f, the distance d between the center of gravity G and the rear axle center point R, the vehicle mass m and the yaw moment of inertia about the center of mass J_{G}.

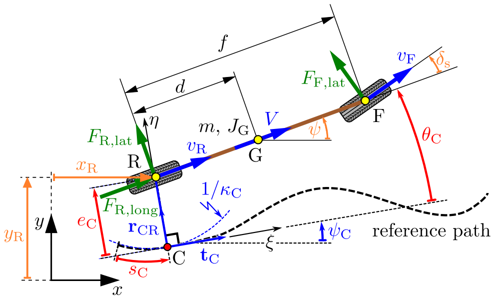

Fig. 1. Vehicle model in path reference frame.

2.1 Vehicle model in the global reference frame

In the global reference frame, we use the coordinates x_{R} and y_{R} of point R, as well as the yaw angle ψ as generalized coordinates to describe the location and orientation of the vehicle. Since no tire side slip is considered in our model, the direction of the velocity vectors at the front and rear axle are determined by the rolling direction of the wheels: at the front (point F), this corresponds to the steering angle δ_{s}, while the velocity vector in point R points into the longitudinal direction. Furthermore, we assume a constant longitudinal speed

V, corresponding to a rear-wheel drive vehicle. These considerations can be described by the following three kinematic constraint equations:

$$\dot{x}_{\mathrm{R}}\sin(\psi+\delta_{\mathrm{s}})-\dot{y}_{\mathrm{R}}\cos(\psi+\delta_{\mathrm{s}})-f\dot{\psi}\cos\delta_{\mathrm{s}}=0, \tag{1}$$

$$-\dot{x}_{\mathrm{R}}\sin\psi+\dot{y}_{\mathrm{R}}\cos\psi=0, \tag{2}$$

$$\dot{x}_{\mathrm{R}}\cos\psi+\dot{y}_{\mathrm{R}}\sin\psi=V. \tag{3}$$

From Eq. (1)–(3), the time derivatives of the generalized coordinates (often called as generalized velocities) can be expressed as

$$\dot{x}_{\mathrm{R}}=V\cos\psi,\quad \dot{y}_{\mathrm{R}}=V\sin\psi,\quad \dot{\psi}=\frac{V}{f}\tan\delta_{\mathrm{s}}\,. \tag{4}$$

In addition, by taking the time derivative of Eq. (4), the acceleration components of point R and the angular acceleration of the vehicle are:

$$\ddot{x}_{\mathrm{R}}=-\frac{V^2}{f}\sin\psi\tan\delta_{\mathrm{s}},\quad \ddot{y}_{\mathrm{R}}=\frac{V^2}{f}\cos\psi\tan\delta_{\mathrm{s}},\quad \ddot{\psi}=\frac{V}{f\cos^2\delta_{\mathrm{s}}}\dot{\delta}_{\mathrm{s}}. \tag{5}$$

Although the tire dynamics are not considered in our vehicle model, we still want to ensure that no loss of traction occurs. This can be verified by calculating the constraint forces acting at the wheels due to the kinematic constraints in Eq. (1)–(3) (denoted by $F_{\mathrm{F,lat}}$, $F_{\mathrm{R,lat}}$ and $F_{\mathrm{R,long}}$ in Fig. 1), and comparing these with the friction limits. We use Lagrange's equations to calculate the constraint forces:

$$\frac{\mathrm{d}}{\mathrm{d}t}\frac{\partial T}{\partial \dot{x}_{\mathrm{R}}}-\frac{\partial T}{\partial x_{\mathrm{R}}}=\nu_1A_{11}+\nu_2A_{21}+\nu_3A_{31}, \tag{6}$$

$$\frac{\mathrm{d}}{\mathrm{d}t}\frac{\partial T}{\partial \dot{y}_{\mathrm{R}}}-\frac{\partial T}{\partial y_{\mathrm{R}}}=\nu_1A_{12}+\nu_2A_{22}+\nu_3A_{32}, \tag{7}$$

$$\frac{\mathrm{d}}{\mathrm{d}t}\frac{\partial T}{\partial \dot{\psi}}-\frac{\partial T}{\partial \psi}=\nu_1A_{13}+\nu_2A_{23}+\nu_3A_{33}, \tag{8}$$

where T is the kinetic energy of the system, ν_1, ν_2 and ν_3 are Lagrange multipliers corresponding to the constraint forces of the three kinematic constraints in Eq. (1)–(3), while A_{ij} $(i,j\in\{1,2,3\})$ are the coefficients of $\dot{x}_{\mathrm{R}}$, $\dot{y}_{\mathrm{R}}$ and $\dot{\psi}$ in Eq. (1)–(3). Namely,

$$A_{11}=\sin(\psi+\delta_{\mathrm{s}}),\quad A_{21}=-\sin\psi,\quad A_{31}=\cos\psi, \tag{9}$$

$$A_{12}=-\cos(\psi+\delta_{\mathrm{s}}),\quad A_{22}=\cos\psi,\quad A_{32}=\sin\psi, \tag{10}$$

$$A_{13}=-f\cos\delta_{\mathrm{s}},\quad A_{23}=0,\quad A_{33}=0. \tag{11}$$

The kinetic energy can be calculated as

$$T=\frac{1}{2}m\left(\dot{x}_{\mathrm{G}}^2+\dot{y}_{\mathrm{G}}^2\right)+\frac{1}{2}J_{\mathrm{G}}\dot{\psi}^2, \tag{12}$$

where the velocity of the center of mass consists of

$$\dot{x}_{\mathrm{G}}=\dot{x}_{\mathrm{R}}-d\dot{\psi}\sin\psi,\quad \dot{y}_{\mathrm{G}}=\dot{y}_{\mathrm{R}}+d\dot{\psi}\cos\psi. \tag{13}$$

Substituting Eq. (9)–(13) into Eq. (6)–(8), the Lagrangian equations read:

$$m(\ddot{x}_{\mathrm{R}} - d\dot{\psi}^2 \cos\psi - d\ddot{\psi} \sin\psi) = \nu_1 \sin(\psi + \delta_{\mathrm{s}}) - \nu_2 \sin\psi + \nu_3 \cos\psi, \quad (14)$$

$$m(\ddot{y}_{\mathrm{R}} - d\dot{\psi}^2 \sin\psi + d\ddot{\psi} \cos\psi) = -\nu_1 \cos(\psi + \delta_{\mathrm{s}}) + \nu_2 \cos\psi + \nu_3 \sin\psi, \quad (15)$$

$$-md\ddot{x}_{\mathrm{R}} \sin\psi + md\ddot{y}_{\mathrm{R}} \cos\psi + (J_{\mathrm{G}} + md^2)\ddot{\psi} = -\nu_1 f \cos\delta_{\mathrm{s}}. \quad (16)$$

Solving Eq. (14)–(16) for the three Lagrange multipliers, then substituting Eq. (4) and (5) leads to

$$\nu_1 = -\frac{V}{2f^2 \cos^3\delta_{\mathrm{s}}} \left(mdV \sin(2\delta_{\mathrm{s}}) + 2(J_{\mathrm{G}} + md^2)\dot{\delta}_{\mathrm{s}} \right), \quad (17)$$

$$\nu_2 = \frac{V}{2f^2 \cos^2\delta_{\mathrm{s}}} \left((f-d)mV \sin(2\delta_{\mathrm{s}}) - 2\left(J_{\mathrm{G}} - (f-d)dm\right) \dot{\delta}_{\mathrm{s}} \right), \quad (18)$$

$$\nu_3 = \frac{V}{f^2 \cos^2\delta_{\mathrm{s}}} (J_{\mathrm{G}} + md^2)\dot{\delta}_{\mathrm{s}} \tan\delta_{\mathrm{s}}. \quad (19)$$

Furthermore, it can be proven using Newton's second law that the Lagrange multipliers correspond to the constraint forces as $F_{\mathrm{F,lat}} = -\nu_1$, $F_{\mathrm{R,lat}} = \nu_2$ and $F_{\mathrm{R,long}} = \nu_3$. Loss of traction will not occur, as long as the constraint forces at the front and rear wheels do not exceed the friction limits, i.e.

$$F_{\mathrm{F,lat}} < \mu_{\mathrm{F}} F_{\mathrm{F},z}, \quad (20)$$

$$\sqrt{F_{\mathrm{R,lat}}^2 + F_{\mathrm{R,long}}^2} < \mu_{\mathrm{R}} F_{\mathrm{R},z}, \quad (21)$$

where μ_{F} and μ_{R} are the coefficients of friction, while $F_{\mathrm{F},z} = mgd/f$ and $F_{\mathrm{R},z} = mg(f-d)/f$ are the vertical wheel loads at the front and rear wheels in steady-state condition, respectively.

2.2 Transformation to path reference frame

In order to design a path following controller, the vehicle model is now transformed to the path reference frame (ξ, η) that moves along the desired path as the vehicle moves forward (see Fig.1). The details of the transformation can be found in [5].

Our control goal is to ensure that the rear axle center point R follows the reference path. Assume that the closest point along the reference path to R is point C. Then the lateral error can be calculated as $e_{\mathrm{C}} = (\mathbf{t}_{\mathrm{C}} \times \mathbf{r}_{\mathrm{CR}}) \cdot \mathbf{k}$, where $\mathbf{t}_{\mathrm{C}}$ is the tangential unit vector to the path in point C, the vector $\mathbf{r}_{\mathrm{CR}}$ points from C to R, and $\mathbf{k}$ is the unit vector normal to the plane of motion. Using the direction ψ_{C} of the tangential vector $\mathbf{t}_{\mathrm{C}}$, the lateral deviation of the vehicle can be expressed as

$$e_{\mathrm{C}} = -(x_{\mathrm{R}} - x_{\mathrm{C}}) \sin\psi_{\mathrm{C}} + (y_{\mathrm{R}} - y_{\mathrm{C}}) \cos\psi_{\mathrm{C}}, \quad (22)$$

while the angle error is

$$\theta_{\mathrm{C}} = \psi - \psi_{\mathrm{C}}. \quad (23)$$

Note that the coordinates x_{C} and y_{C} of point C, the angle ψ_{C} as well as the curvature κ_{C} of the reference path in point C all depend on the arc length s_{C} and are assumed to be given. The transformation from the absolute position and orientation of the vehicle $(x_{\mathrm{R}}, y_{\mathrm{R}}, \psi)$ to the relative position and orientation $(s_{\mathrm{C}}, e_{\mathrm{C}}, \theta_{\mathrm{C}})$ with respect to the reference path can be performed as

$$\dot{s}_{\mathrm{C}} = \frac{\cos\psi_{\mathrm{C}}}{1-\kappa_{\mathrm{C}}e_{\mathrm{C}}}\dot{x}_{\mathrm{R}} + \frac{\sin\psi_{\mathrm{C}}}{1-\kappa_{\mathrm{C}}e_{\mathrm{C}}}\dot{y}_{\mathrm{R}}, \tag{24}$$

$$\dot{e}_{\mathrm{C}} = -\dot{x}_{\mathrm{R}}\sin\psi_{\mathrm{C}} + \dot{y}_{\mathrm{R}}\cos\psi_{\mathrm{C}}, \tag{25}$$

$$\dot{\theta}_{\mathrm{C}} = -\frac{\kappa_{\mathrm{C}}\cos\psi_{\mathrm{C}}}{1-\kappa_{\mathrm{C}}e_{\mathrm{C}}}\dot{x}_{\mathrm{R}} - \frac{\kappa_{\mathrm{C}}\sin\psi_{\mathrm{C}}}{1-\kappa_{\mathrm{C}}e_{\mathrm{C}}}\dot{y}_{\mathrm{R}} + \dot{\psi} \tag{26}$$

(see [5] for details). Substituting the equations of the kinematic vehicle model (Eq. (4)) results in

$$\dot{s}_{\mathrm{C}} = \frac{V\cos\theta_{\mathrm{C}}}{1-\kappa_{\mathrm{C}}e_{\mathrm{C}}}, \tag{27}$$

$$\dot{e}_{\mathrm{C}} = V\sin\theta_{\mathrm{C}}, \tag{28}$$

$$\dot{\theta}_{\mathrm{C}} = \frac{V}{f}\tan\delta_{\mathrm{s}} - \frac{V\kappa_{\mathrm{C}}\cos\theta_{\mathrm{C}}}{1-\kappa_{\mathrm{C}}e_{\mathrm{C}}}, \tag{29}$$

where the first equation describes the longitudinal motion of point C as it moves along the reference path, while the remaining two equations correspond to the evolution of the lateral deviation and the angle error of the vehicle. Note that since the curvature κ_{C} depends on the arc length s_{C}, all three equations are coupled. In the following, the transformed equations will be used to design a path-following controller.

3 Path-following control

In order to ensure that the rear axle center point can follow the reference path, the steering angle of the vehicle will be generated using the combination of a feedforward term $\delta_{\mathrm{s}}^{\mathrm{FF}}$ and a stabilizing feedback term $\delta_{\mathrm{s}}^{\mathrm{FB}}$:

$$\delta_{\mathrm{s}}(t) = \delta_{\mathrm{s}}^{\mathrm{FF}} + \delta_{\mathrm{s}}^{\mathrm{FB}}. \tag{30}$$

Based on the kinematics of the vehicle in Eq. (27)–(29), the ideal steering angle to follow a reference path of curvature κ_{C} with zero position and angle error is

$$\delta_{\mathrm{s}}^{\mathrm{FF}} = \arctan\left(\kappa_{\mathrm{C}} f\right), \tag{31}$$

while the feedback controller is designed with the proportional feedback of the error terms e_{C} and θ_{C}:

$$\delta_{\mathrm{s}}^{\mathrm{FB}}(t) = -P_e e_{\mathrm{C}}(t-\tau) - P_\theta\theta_{\mathrm{C}}(t-\tau). \tag{32}$$

The control gains are denoted by P_e and P_θ, and we also consider the time delay τ in the feedback loop, which includes sensing and communication delays, signal processing time as well as actuator delays.

4 Stability analysis

In the following, we perform the linear stability analysis of the closed-loop system consisting of the vehicle model in path reference frame (Eq. (27)–(29)) and the path following controller defined in Eq. (30)–(32). The stability analysis is performed for the case of constant path curvature ($\kappa_{\mathrm{C}} = \text{const.}$). Moving along the reference path with zero error and a constant speed V corresponds to the steady state $s_{\mathrm{C}} = Vt$, $e_{\mathrm{C}} \equiv 0$ and $\theta_{\mathrm{C}} \equiv 0$. After linearizing the closed-loop system around this steady state, the equation of s_{C} can be decoupled from the rest (i.e. the longitudinal and lateral dynamics can be treated separately), leading to the linear model

$$\dot{\mathbf{x}}(t) = \mathbf{A}\mathbf{x}(t) + \mathbf{B}\mathbf{K}\mathbf{x}(t-\tau), \tag{33}$$

where the state vector is $\mathbf{x} = \begin{bmatrix} e_{\mathrm{C}} \; \theta_{\mathrm{C}} \end{bmatrix}^{\mathrm{T}}$, the control gains are collected into $\mathbf{K} = \begin{bmatrix} -P_e \; -P_\theta \end{bmatrix}$, and the system and input matrices are

$$\mathbf{A} = \begin{bmatrix} 0 & V \\ -V\kappa_{\mathrm{C}}^2 & 0 \end{bmatrix}, \quad \mathbf{B} = \begin{bmatrix} 0 \\ \frac{V}{f} + Vf\kappa_{\mathrm{C}}^2 \end{bmatrix}. \tag{34}$$

Using an exponential trial function, the characteristic equation of the controlled vehicle can be reached as

$$D(\lambda) := \det\left(\lambda\mathbf{I} - \mathbf{A} - \mathbf{B}\mathbf{K}\mathrm{e}^{-\lambda\tau}\right) = 0, \tag{35}$$

where $\lambda = \rho + \mathrm{i}\omega$ is the (complex) characteristic exponent and $\mathbf{I}$ is the identity matrix. After substitution, the characteristic function reads:

$$D(\lambda) = \lambda^2 + \frac{1}{f}P_\theta V\left(1 + f^2\kappa_{\mathrm{C}}^2\right)\lambda\mathrm{e}^{-\lambda\tau} + V^2\left(\frac{P_e}{f} + P_e f\kappa_{\mathrm{C}}^2\right)\mathrm{e}^{-\lambda\tau} + V^2\kappa_{\mathrm{C}}^2. \tag{36}$$

Because of the time delay in the system, the characteristic equation is transcendental in λ, and the stability analysis can be performed using e.g. the D-subdivision method [6]. At the boundaries of stability loss, the critical characteristic exponent will be purely imaginary, e.g. $\lambda = \mathrm{i}\omega$. If $\omega = 0$, static stability loss occurs, which can happen at the stability boundary $D(\lambda = 0) = 0$, i.e.

$$P_e = -\frac{f\kappa_{\mathrm{C}}^2}{1 + f^2\kappa_{\mathrm{C}}^2}. \tag{37}$$

Notice that for $\kappa_{\mathrm{C}} = 0$, this corresponds to $P_e = 0$, but for non-zero path curvature, the stability limit moves into the negative region of P_e.

The boundaries of dynamic stability loss can be analyzed by separating the real and imaginary parts of the equation $D(\lambda = \mathrm{i}\omega) = 0$. Solving the resulting two equations for the control gains P_e and P_θ leads to the stability boundaries in the (P_e, P_θ) plane:

$$P_e(\omega) = \frac{f(\omega^2 - V^2\kappa_{\mathrm{C}}^2)\cos(\omega\tau)}{V^2(1 + f^2\kappa_{\mathrm{C}}^2)}, \quad P_\theta(\omega) = \frac{f(\omega^2 - V^2\kappa_{\mathrm{C}}^2)\sin(\omega\tau)}{V(1 + f^2\kappa_{\mathrm{C}}^2)\omega}. \tag{38}$$

Table 1. Vehicle parameters used in stability charts and numerical simulations

f (m)	d (m)	m (kg)	J_{G} (kgm^2)	V (m/s)	τ (s)	μ_{F}	μ_{R}
2.7	1.35	1430	2500	20	0.5	1	1

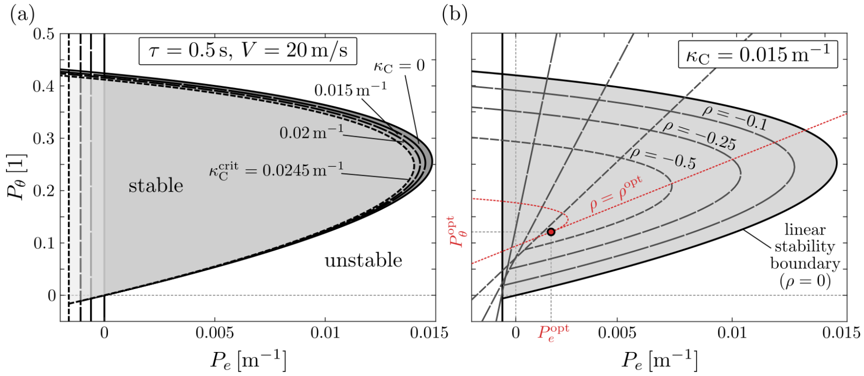

Fig. 2. (a) The stable domain of control gains for different values of path curvature κ_{C}. (b) Contourlines of the real part of the rightmost characteristic exponent along the stable domain. The red dot denotes the optimal gain combination that leads to the fastest decay of small oscillations.

The stable domain is enclosed by the stability boundary as shown in Fig. 2(a) for the vehicle parameters in Table 1. It can be seen that increasing the path curvature κ_{C} leads to a slight shift in the location of the stable domain towards the negative control gain directions. However, even if the path curvature reaches the critical value $\kappa_{\mathrm{C}}^{\mathrm{crit}}$, where the steady state tire forces exceed the friction limits (as defined in Eq. (20) and (21)), the change in the stable domain of control gains is not very significant.

To check how the performance of the controller changes by varying the two control gains inside the stable domain, the above calculations can be repeated by also taking into account the real part ρ of the critical characteristic exponent, which corresponds to the decay rate of small oscillations. Figure 2(b) shows the contour lines inside the stable domain that correspond to a given value of ρ. Similarly to the boundaries of static and dynamic stability loss, the contour lines for a given value of $\rho < 0$ can be separated into a straight line where $\omega = 0$ (i.e. the critical characteristic exponent is $\lambda_{\mathrm{cr}} = \rho$) and a curve where $\omega > 0$ (i.e. $\lambda_{\mathrm{cr}} = \rho \pm \mathrm{i}\omega$). The best control performance can be achieved when the value of ρ is minimized, which occurs if the slope of the straight contour line corresponding to $\omega = 0$ is equal to the initial slope of the curve, i.e. there is no enclosed area between the two. The real part of the critical characteristic exponent in this case is

$$\rho^{\mathrm{opt}} = \frac{1}{\tau^2}\left(-2\tau + \sqrt{2\tau^2 - V^2\kappa_{\mathrm{C}}^2\tau^4}\right), \tag{39}$$

and the corresponding optimal control gains can be calculated as

$$P_e^{\mathrm{opt}} = \frac{2f\mathrm{e}^{-2+\sqrt{2-V^2\kappa_{\mathrm{C}}^2\tau^2}}\left(-7 + V^2\kappa_{\mathrm{C}}^2\tau^2 + 5\sqrt{2-V^2\kappa_{\mathrm{C}}^2\tau^2}\right)}{V^2(1+f^2\kappa_{\mathrm{C}}^2)\tau^2}, \tag{40}$$

$$P_\theta^{\mathrm{opt}} = \frac{2f\mathrm{e}^{-2+\sqrt{2-V^2\kappa_{\mathrm{C}}^2\tau^2}}\left(-1 + \sqrt{2-V^2\kappa_{\mathrm{C}}^2\tau^2}\right)}{V(1+f^2\kappa_{\mathrm{C}}^2)\tau}. \tag{41}$$

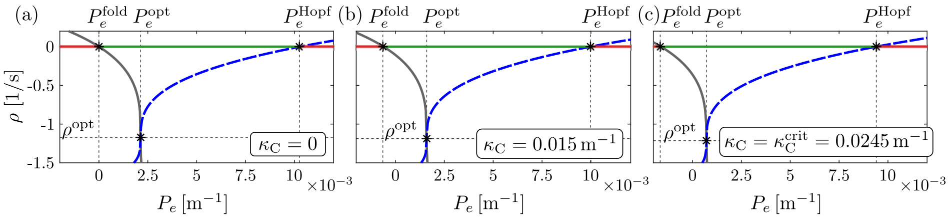

Fig. 3. The real parts of the rightmost characteristic exponents as a function of the control gain P_e for different values of path curvature κ_{C}. Black continuous and blue dashed lines represent real and complex conjugate pairs of characteristic roots, respectively. The color of the stability boundary $\rho = 0$ indicates the stable (green) and unstable (red) ranges of P_e. The value of P_θ is set as the optimum in each panel, as follows: (a) $P_\theta = 0.1245$, (b) $P_\theta = 0.1210$, (c) $P_\theta = 0.1151$.

Figure 3 shows the real parts of the rightmost characteristic roots as the control gain P_e is varied, for three different values of path curvature. In each panel, the value of P_θ is fixed to the optimum P_θ^{opt}, calculated using the corresponding path curvature κ_{C}. It can be seen that at the boundary of static loss of stability (P_e^{fold}), a real characteristic exponent crosses the imaginary axis (black curves), while at the boundary of dynamic stability loss (P_e^{Hopf}), a complex conjugate pair of roots move to the right half plane (blue dashed lines), leading to a Hopf bifurcation in the nonlinear system. The best control performance can be achieved by selecting the control gain P_e^{opt}, where the real and the complex conjugate pair of roots merge.

The root tendencies in Fig. 3 show that as the path curvature is increased, the optimal gain P_e^{opt} decreases. Additionally, if the controller is tuned with the assumption of a straight-line reference path (using the optimal gains in Fig. 3(a)), then as the path curvature increases (while the control parameters remain fixed), the rightmost roots will move closer to the imaginary axis, leading to a decrease in control performance.

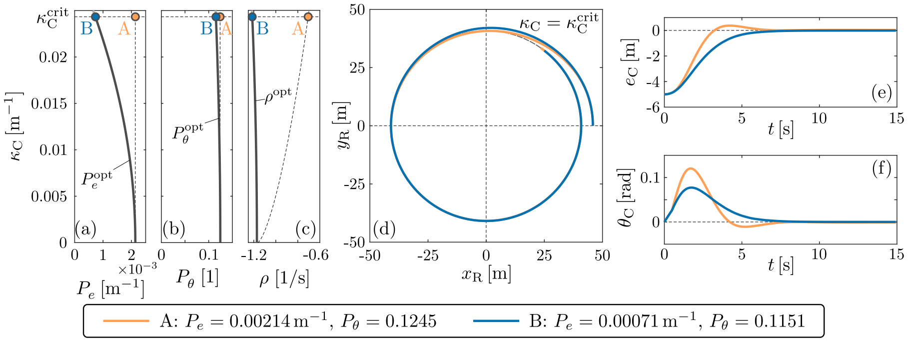

Fig. 4. The optimal control gains (panels (a) and (b)) and the real part of the rightmost characteristic exponent (panel (c)) as the path curvature is increased. Panels (d)-(f): numerical simulations with (point B) and without (point A) taking into account the path curvature when tuning the controller.

This effect is further illustrated in Fig. 4. Panels (a) and (b) show how the optimal control gains change as the path curvature increases from zero to κ_C^{crit}, where loss of traction occurs in steady state. It can be seen that the location of P_θ^{opt} is not very sensitive to the path curvature, but the optimal value of P_e decreases to less than its third until κ_C^{crit} is reached. In panel (c), the real part of the rightmost characteristic root is plotted for increasing path curvatures, assuming an optimally tuned controller. This indicates that as long as the control gains are adjusted, the path curvature does not affect control performance significantly. On the other hand, the dashed line in panel (c) shows that if the optimal gains corresponding to $\kappa_C = 0$ are used regardless of path curvature, the rightmost roots will move closer to the imaginary axis as κ_C is increased, and control performance will degrade.

A pair of numerical simulations using the nonlinear vehicle model are shown in panels (d)-(f) (vehicle parameters are listed in Table 1). In order to better illustrate the effect of properly tuning the controller, the reference path is chosen to be a circle of curvature κ_C^{crit} (we note that transients are not accounted for in our calculations of determining the critical path curvature, therefore this choice would be highly unsafe in practice). In the orange trajectory (point A in panels (a)-(c)), the optimal control gains for $\kappa_C = 0$ are selected, while in the blue trajectory (point B), the gains have been adjusted according to the reference path. It can be seen that if the control gains are not adjusted, some overshoot will appear in the system response, while using the properly tuned optimal gains leads to a visibly smoother trajectory. Under normal driving conditions, the difference would mainly affect passenger comfort, but in highly dynamic, safety critical maneuvers, the difference in overshoot might determine whether loss of traction occurs or not.

5 Conclusion

The stability analysis of a path following controller with feedback delay was performed in this paper, with the consideration of the curvature of the reference path. Using a simple, kinematic vehicle model, analytical expressions have been derived for the stability boundaries and the optimal control gains in terms of the fastest decay of the linearized system. Using stability charts and numerical simulations, we showed that taking into account the path curvature when tuning the controller leads to smoother path following without overshoot. This improves passenger comfort and allows performing a wider range of emergency maneuvers.

The main limitation of the current study is that tire behavior and loss of traction was only indirectly taken into account, therefore the results should be verified using a higher fidelity vehicle model too, especially if highly dynamic maneuvers are considered.

6 Acknowledgment

The research was partly supported by a János Bolyai Research Scholarship of the Hungarian Academy of Sciences and by the National Research, Development and Innovation Office of Hungary (grants no. NKFI-128422 and 2020-1.2.4-TÉT-IPARI-2021-00012), as well as by the ÚNKP-22-3-II-BME-116 New National Excellence Program of the Ministry for Culture and Innovation from the source of the National Research, Development and Innovation Fund.

References

1. Paden, B., Čáp, M., Yong, S. Z., Yershov, D., Frazzoli, E. (2016) A survey of motion planning and control techniques for self-driving urban vehicles. *IEEE Transactions on Intelligent Vehicles*, **1**(1):33-55.
2. Mastinu, G., Biggio, D., Della Rossa, F., Fainello, M. (2020) Straight running stability of automobiles: experiments with a driving simulator. *Nonlinear Dynamics*, **99**(4), 2801-2818.
3. Yang, L., Yue, M., Ma, T. (2019) Path following predictive control for autonomous vehicles subject to uncertain tire-ground adhesion and varied road curvature. *International Journal of Control, Automation and Systems*, **17**(1):193-202.
4. Vörös, I., Takács, D. (2022) Lane-keeping control of automated vehicles with feedback delay: Nonlinear analysis and laboratory experiments. *European Journal of Mechanics-A/Solids*, **93**, 104509.
5. Qin, W. B., Zhang, Y., Takács, D., Stépán, G., Orosz, G. (2022) Nonholonomic dynamics and control of road vehicles: moving toward automation. *Nonlinear Dynamics*, 1-46.
6. Insperger, T., Stépán, G.: Semi-discretization for time-delay systems: stability and engineering applications. Springer Science & Business Media (2011)